Available online at www.sciencedirect.com
SCIENCE DIRECT®
Journal of the European Ceramic Society 25 (2005) 1293–1299
www.elsevier.com/locate/jeurceramsoc

Self assemble silicide architectures by directional solidification

F.W. Dynys [a, *], A. Sayir [a, b]

[a] NASA-Glenn Research Center, 21000 Brookpark Road, Cleveland, OH 44135, USA
[b] Case Western Reserve University, 21000 Brookpark Road, Cleveland, OH 44135, USA

Available online 21 February 2005

Abstract

Directional solidification of eutectics has self assembly characteristics that can fabricate two dimensional periodic arrays of two or more phases. The ordering of the phases can be utilized as a "lithographic technique" to produce porous structures for fabrication of miniature devices. Directional solidification by the Bridgman technique was applied to the eutectic systems Si–$TiSi_2$ and Si–YSi_2. Patterned growth of $TiSi_2$ rods occur in the silicon matrix during solidification. Micro-channel structure of pillar arrays of $TiSi_2$ was produced by silicon dissolution by KOH. Average $TiSi_2$ rod diameter was 2.5 μm with 99% of the population falling in the 2–3 μm range. Colony formation could not be suppressed in the Si–$TiSi_2$ system. Patterned growth is not observed in Si–YSi_2 system. Eutectic and hyper-eutectic Si–YSi_2 compositions formed anomalous eutectic microstructure. Microstructure shows dependence upon the solidification rate.

Keywords: Silicides; Composite; Microstructure-final

1. Introduction

In recent years, there has been growing interest in the fabrication of two dimensionally ordered porous materials consisting of honeycomb structures, pillar/pin arrays or linear channels, as illustrated in Fig. 1. The ordering dimension ranges from the micrometer to nanometer scale. The long range ordering of the pores, pillars and channels result in useful characteristics such as photonic bandgaps, high packing density and high surface to volume ratio. Potential applications range from information processing and storage, separation membranes, sensor arrays, catalysis, propulsion technology, wave guides, heat exchanger, embossing tool and bio-medical devices. As NASA enters the era in small spacecraft technology[1] and planetary exploration, miniaturization and mass reduction of components will be viable.

The need for compact, lightweight and efficient chemical and fuel processing devices has lead to micro-process technology.[2] Micro-process technology involves minimizing the characteristic internal dimensions of reactors and heat exchangers to enhance heat and mass transfer. All elements of traditional chemical processes can be achieved using microtechnology, heat exchangers, reactors, and separators can be miniaturized. Chemical processing will be viable in converting planetary resources into propellants, oxygen, water and other useful chemicals.

Silicon has been a natural candidate material for testing micro-channel devices because of the matured microfabrication technology. Aeronautic operating environments will require materials capable to perform at higher temperatures under harsh chemical environments than silicon can sustain. Lithography technology is immature for most non-silicon based materials. Directional solidification of the eutectic (DSE) offers an alternative pathway to fabricate patterned structures. DSE has self-assembly characteristics that can fabricate two-dimensional periodic arrays of two or more phases by crystallization from the melt. The size and periodic spacing of rods or lamella normally range from 100 nm to 100 μm. Porous structures with high aspect ratios can be achieved by phase removal. DSE as a "lithographic technique" has been investigated for metallic and ceramic systems by Cline,[3] Angers et al.,[4] Ditchek and Emma,[5] and Orera et al.[6,7] Thermionic emitter arrays have been successfully fabricated using DSE.[8,9] This paper reports work on DSE as a lithographic technique for the eutectic systems Si–$TiSi_2$ and Si–YSi_2. The Si–$TiSi_2$ system was selected because it

* Corresponding author.

0955-2219/$ – see front matter © 2005 Published by Elsevier Ltd.
doi:10.1016/j.jeurceramsoc.2005.01.033

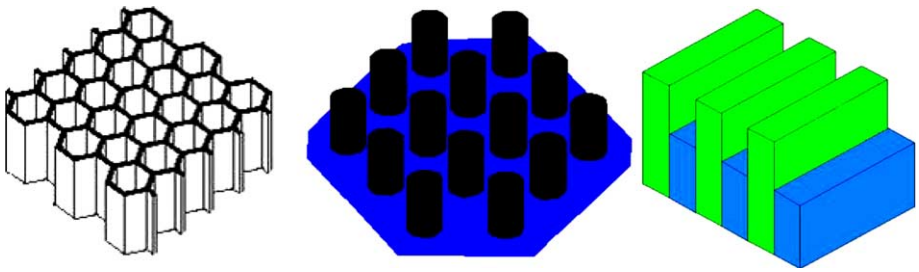

Fig. 1. Two dimensional ordered pore structures.

exhibits patterned growth of $TiSi_2$ rods. Relationship of microstructure with processing parameters will be discussed along preliminary results on etching of the phases.

2. Experimental procedure

Starting materials for ingot preparation were metallic elements of commercial purity, ≥99.9%. The silicon alloy compositions investigated are shown in Table 1. Boron nitride crucibles were used containing 30–40 g of the silicon alloy composition. Compositions were melted in an argon atmosphere in a graphite resistance heated furnace. Temperature was controlled by an optical pyrometer. Table 1 shows the melt temperature for each composition. Alloy compositions were soaked at melt temperatures for 4–5 h to achieve homogenization. Furnace power was turned off to rapidly quench the alloy composition.

The directional growth of eutectic, hyper-eutectic and hypo-eutectic compositions was accomplished using the vertical Bridgman method. Pull rate and melt temperature for each composition is given in Table 1. The temperature gradient was 8.5 °C/mm. Ingots were approximately 20 mm is length and 22 mm in diameter.

The crystalline phases were determined by X-ray diffraction. The X-ray diffractometer was equipped with a Cu Kα source with a wavelength of 0.1540 nm. The operating conditions were 45 kV and 40 mA. Scans were conducted at 3°/min with a sampling interval of 0.02°.

The BN crucible is reactive to titanium, this has been noted by Crossman and Yue[10] for Ti–Ti_5Si_3 system. Attempts using Al_2O_3 crucibles were not successful because they mechanically failed during solidification. The BN crucibles were sufficient in containing the melt under these process conditions.

Faceted precipitates of TiB_x are observed near the crucible interface. It is probable that the melt is contaminated with a small level of boron. There was no apparent interaction between the precipitates and the eutectic microstructure.

Table 1
Solidification conditions

Alloy	Si (wt.%)	Temperature (°C)	Pull rate (mm/h)
Ti-eutectic	75	1525	130, 30, 6
Ti-hyper-eutectic	70	1525	30, 6
Ti-hyper-eutectic	80	1525	30, 6
Ti with 1 wt.% Mo	74.5	1575	120
Ti with 1 wt.% Zr	74.5	1575	120
Y-eutectic	59	1575	30, 8
Y-hyper-eutectic	55	1575	8
Y-hyper-eutectic	50	1575	8
Y-hyper-eutectic	45	1575	8

3. Results

3.1. Si–$TiSi_2$

The understanding of the microstructural development of the eutectic systems is critical to control the pore or channel dimensions. It was found that formation of $TiSi_2$ rods occurs naturally in the Si–$TiSi_2$ system. Non-directional solidification of the melt in an Al_2O_3 crucible produces colonies containing $TiSi_2$ rods. The colonies containing $TiSi_2$ rods are randomly oriented. It should be noted that $TiSi_2$ rods formed in the absence of boron contamination.

Directional solidification was employed along the thermal gradient to promote homogeneous rods or lamellae structure. The spacing of the rods or lamellae is dependent upon rate of solidification (R) and thermal gradient (G). The eutectic composition containing 75 wt.% Si was solidified at rates of 130, 30 and 6 mm/h. Phase analysis of the specimens by X-ray diffraction showed the expected phases, Si and $TiSi_2$. Fig. 2 shows a transverse and longitudinal micrograph of the Si–$TiSi_2$ eutectic solidified at 6 and 30 mm/h, respectively. Large colonies, >100 m, containing $TiSi_2$ rods are observed. $TiSi_2$ rods are not preferentially orientated along the thermal gradient. The boundary structure between colonies is irregular and contains coarser precipitates. The higher solidification rates do not significantly change the microstructure; it tends to produce larger size colonies. Similar microstructures are observed for the hyper-eutectic and hypo-eutectic compositions. A small addition of Zr and Mo were added to the eutectic composition to promote change in the microstructure by changing the interfacial energy. $ZrSi_2$ is isostructural with $TiSi_2$. Fig. 3 shows the transverse microstructure of 1 wt.% Zr addition solidified at 120 mm/h. The results indicate no solid solution between $ZrSi_2$ and $TiSi_2$. Using back scattered electrons (BSE), microstructure examination reveals $ZrSi_2$ precipitation at the colony bodies. The $ZrSi_2$ precipitates have same morphology as observed in directionally solidified mi-

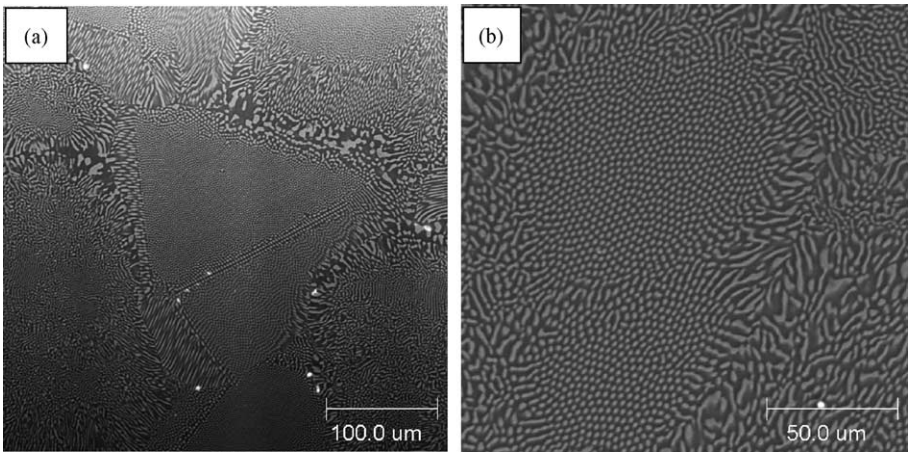

Fig. 2. Microstructure of directionally solidified Si–$TiSi_2$ eutectic composition: (a) transverse section at 6 mm/h and (b) longitudinal section at 30 mm/h.

crostructures of the eutectic system Si–$ZrSi_2$. The addition of Zr enhances colony formation. The expectation for Mo addition was solubility in Si. Fig. 4 shows the transverse microstructure of 1 wt.% Mo addition solidified at 120 mm/h. BSE imaging shows large precipitates containing Mo. Examination of the microstructure indicates no apparent interaction between the eutectic microstructure and Mo containing precipitates. The addition of Mo and Zr did change the crystallization behavior of $TiSi_2$ rods (Fig. 5).

The observed microstructures may be examined using Hunt and Jackson criteria. Hunt and Jackson[11] developed a method to predict eutectic microstructures based upon entropy of fusion. The eutectic structure will exhibit a regular morphology (rod-like or lamellar) if both phases possess low entropy of fusion, typically, $\Delta S/R < 2$, where ΔS is the entropy of fusion and R is the gas constant. For the Si–$TiSi_2$ system, both the Si phase and $TiSi_2$ have high entropies of fusion; ΔS_{Si} is 30 J/K mol[12] and ΔS_{TiSi_2} is ~54 J/K mol.[13] Both phases have high value of $\Delta S/R > 2$. The expected microstructure based on Hunt and Jackson criteria would be the irregular (faceted for both faces) structure. In contrary to this expectation, Fig. 2 depicts a "complex regular" microstructure which has many of the features of fibrous eutectic microstructure within the colonies. This apparent contradiction could be explained through the stabilization of isothermal liquid–solid interface through kinetic undercooling. In high entropy melting Si–$TiSi_2$ system, the kinetic undercooling of $TiSi_2$ phase is large. In this case, the kinetic undercooling can balance the undercooling due to composition undercooling providing local isothermal interface and consequently leading to rod-like structure formation. This has been also observed for eutectic (75 wt.% Si) and off-eutectic compositions (70 and 80 wt.% Si). At eutectic invariant point, the starting composition is expected to yield volume fraction of minor phase of 31 vol.% Si phase. However, the eutectic composition became Si rich by depletion of Ti through the reac-

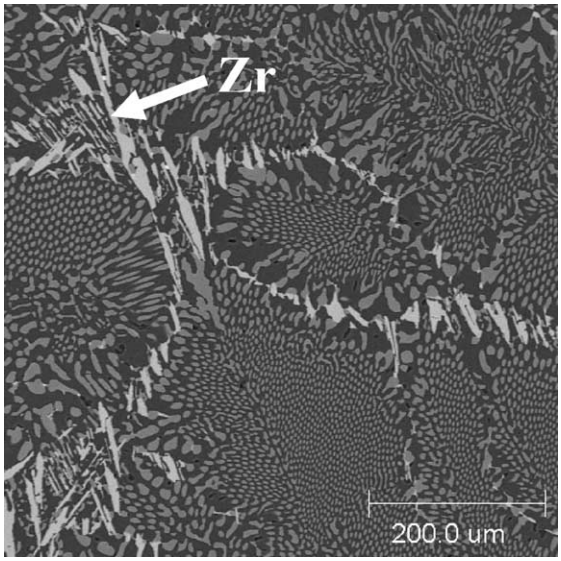

Fig. 3. Back scatter electron micrograph of Si–$TiSi_2$ eutectic with 1 wt.% Zr.

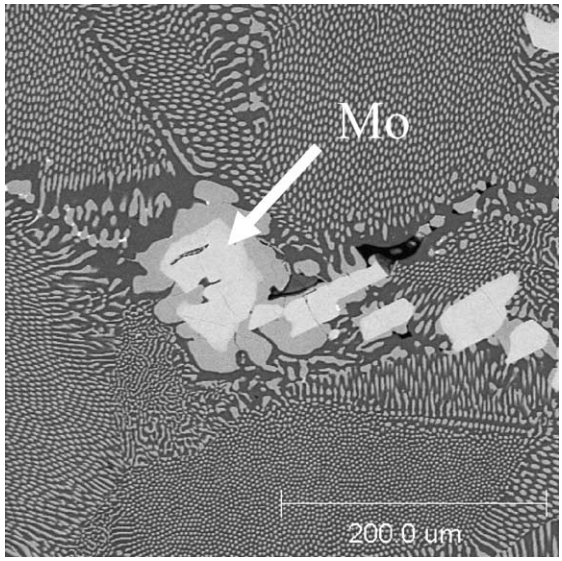

Fig. 4. Back scatter electron micrograph of Si–$TiSi_2$ eutectic with 1 wt.% Mo.

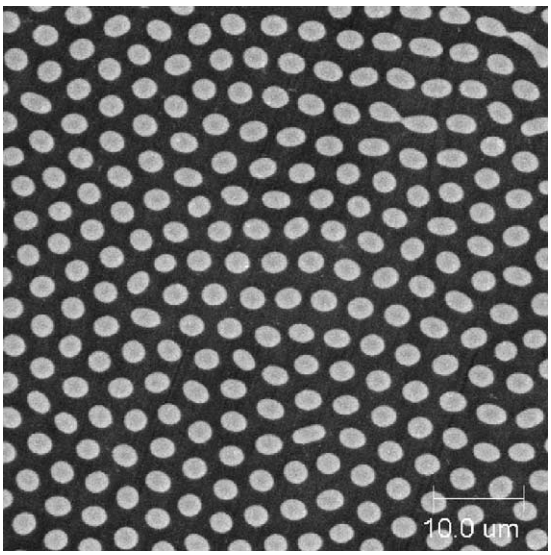

Fig. 5. $TiSi_2$ rods in a Si matrix.

tion of BN crucible with the melt. The amount and spatial distribution of boron and its effect on the stabilization of the liquid–solid isotherm needs further study. Constitutional undercooling due to boron buildup can stabilize the cellular interface producing cellular microstructure, Fig. 2. Current efforts are focusing to attain homogeneous $TiSi_2$ rod-like structures using controlled amount dopant additions under high G/R ratio and inhibiting colony formation.

A significant aspect of eutectic growth under directional conditions is the relationship between solidification rate (R) and inter-rod spacing (λ). A common observation is that $\lambda^2 R$ = constant. Table 2 shows the dependence of inter-rod spacing on solidification rate, suggesting a linear relationship of λR = constant. Theoretically, however, for a given lamella spacing, a range of growth rates is possible[14] and we did not made any attempt to assign specific relation ship between the solidification rate (R) and inter-rod spacing (λ). Normally, the spacing (λ) for other material systems shows a larger dependence upon solidification rate. The mean $TiSi_2$ rod diameter is 2.5 μm as shown in Fig. 6. The size ranges from 2 to 3 μm, 99% of the rods fall into this size range.

Chemical etching was performed on polished specimens using KOH solution. A 5 min soak at 80 °C in a 10 M KOH solution was sufficient to etch the silicon. Fig. 7 shows that a pillar array of $TiSi_2$ can be readily fabricated. It was observed that there was a minor population where there was deep undercutting at the $TiSi_2$–Si interface. It was not determined if the undercutting was caused by cracks, impurity segregation or some other unknown cause. A selective wet

Table 2
$TiSi_2$ inter-rod spacing

Solidification rate (mm/h)	Spacing (Δm)
6	5.7
30	5.6
130	4.3

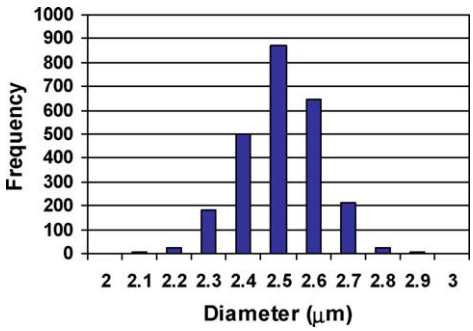

Fig. 6. Diameter distribution of $TiSi_2$ rods.

chemical etch for $TiSi_2$ was not found in the literature.[15] Plasma etching was performed to evaluate its effectiveness using a CF_4/O_2 mixture. Fig. 8 shows the etched microstructure. The sample was polished prior to the dry plasma etch. Selective etching is observed around the Si–$TiSi_2$ interface. Craters form around the $TiSi_2$ rods. A minor population of $TiSi_2$ rods exhibit non-uniform etching where deep channels are observed. The $TiSi_2$ etches in facet geometry, some are pyramidal in shape. The etched chemistry used enhances fluorine concentration in the plasma. The opportunity exists to change the plasma chemistry to promote passivating films to control etching.[16] Forthcoming experiments will explore this etch chemistry.

3.2. Si–YSi_2

The series of representative SEM micrographs demonstrate the microstructural development as a function of composition and solidification rate. For both solidification rates the distinguishing feature was the lack of well-defined microstructure for all compositions investigated. The structures

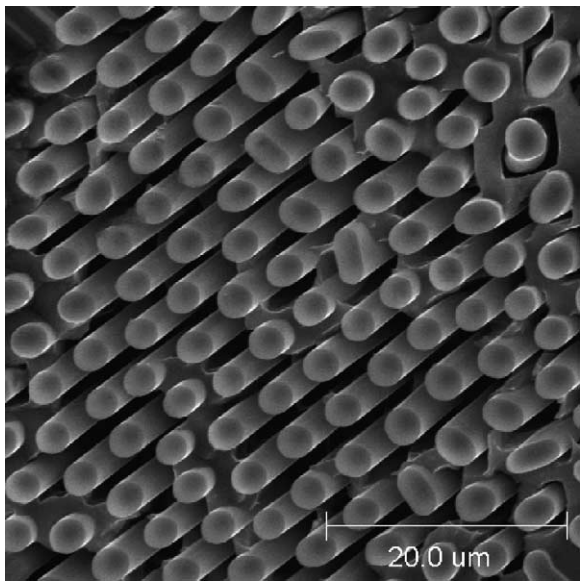

Fig. 7. Exposed $TiSi_2$ rods by KOH etching.

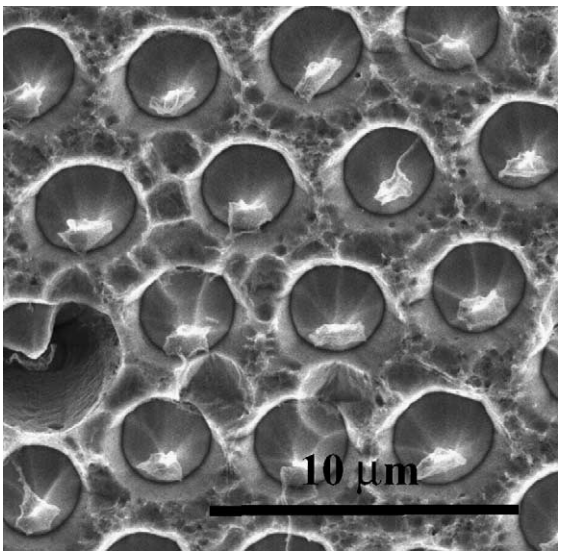

Fig. 8. Plasma etched Si–$TiSi_2$ microstructure.

were irregular with very little indication for a preferred ordering of the phases. Hence, the eutectic structure of the Si–YSi_2 system appeared to be an anomalous eutectic for all hyper-eutectic compositions. The structure of eutectic composition differed especially at the high solidification rate.

The solidification of Si–YSi_2 system at the eutectic composition produced two distinct microstructures at different pull rates at a constant temperature gradient. A pull rate of 130 mm/h produces irregular lamella of alternating Si and YSi_2 phases as shown in Fig. 9. The structure is almost free of primary phase, infrequent needle shaped Si-precipitates are observed as a primary phase. Changing the pull rate to a slower rate alters the crystallized microstructure as shown in Fig. 10. A rate of 8 mm/h produces primary precipitation

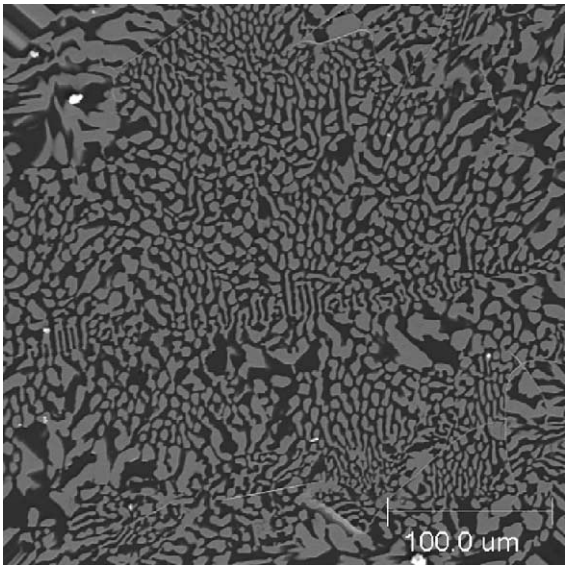

Fig. 9. Microstructure of directionally solidified Si–YSi_2 eutectic at 130 mm/h.

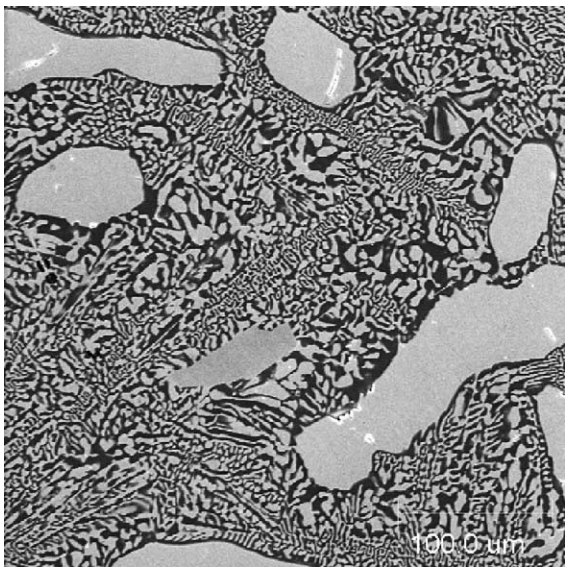

Fig. 10. Microstructure of directionally solidified Si–YSi_2 eutectic at 8 mm/h.

of YSi_2 phase followed by secondary crystallization of the eutectic. Under a constant temperature gradient, different microstructures indicate that there is a characteristic relationship Si phase and YSi_2 phase. A slow pull rate indicates that the growth velocity of YSi_2 phase is greater than the eutectic, $V_{YSi_2}^{primary} > V_{eut}$, and the planar interface is unstable. A higher pull rate suggests that planar growth is stable for the cellular eutectic interface; hence $V_{eut} > V_{YSi_2}^{primary}$ and $V_{eut} > V_{Si}^{primary}$. The solidification front, especially at the central portion of the melt, occasionally promotes the condition where $V_{Si}^{primary} > V_{eut}$ and Si phase precipitates as a primary phase with a needle geometry.

X-ray diffraction revealed that the high temperature form YSi_2 and Si are the crystalline phases. Comparison of the X-ray diffraction patterns show that (1 1 1) Si orientation and the (0 0 1) YSi_2 orientation are absented for the 130 mm/h sample. The 8 mm/h sample also had a minor unknown diffraction peak with a *d*-spacing of 0.1582 nm. The Y_3Si_5 phase matches the unknown diffraction peak, suggesting the presence of Y_3Si_5. The observation suggests possible crystal orientation relationship between phases during a large constitutional undercooling. Determination of crystal growth habits was not integral to this investigation.

The solidification of Si–YSi_2 alloy at hyper-eutectic compositions are shown in Fig. 11. The hyper-eutectic compositions were pulled at 8 mm/h. Compositions of 50 and 55 wt.% silicon nucleate crystals of the high melting point phase YSi_2. Thus, these hyper-eutectic compositions exhibit $V_{YSi_2}^{primary} > V_{eut}$. These hyper-eutectic compositions along with the eutectic composition exhibit a microstructure consisting of primary YSi_2 precipitates with secondary nucleation of the eutectic structure. The Si phase in the hyper-eutectic region is thought to nucleate on the precipitated YSi_2 and grow to envelope the precipitated YSi_2 phase. This

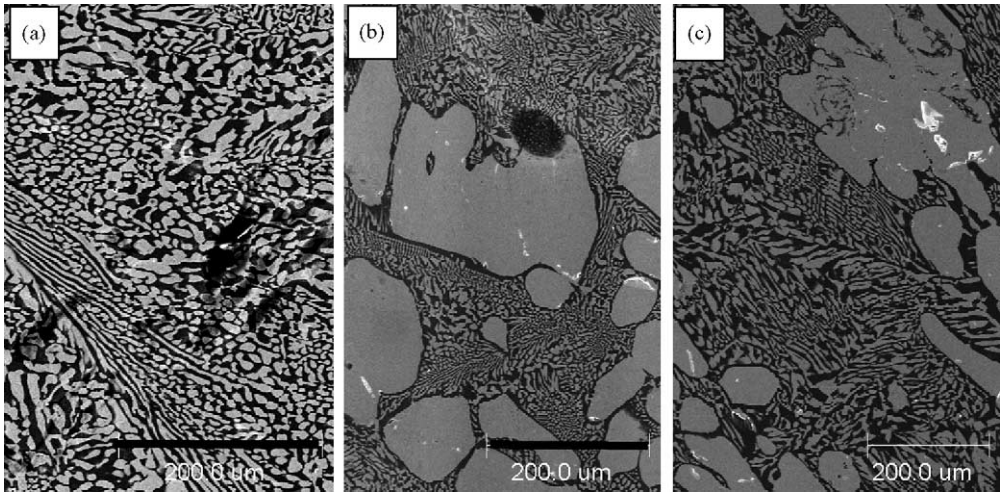

Fig. 11. Microstructures of directionally solidified Si–YSi_2 hyper-eutectics at 8 mm/h: (a) 45 wt.% Si, (b) 50 wt. % Si and (c) 55 wt.% Si.

changes the liquid composition towards the eutectic composition and re-nucleates the YSi_2 phase. The Si phase as a minor phase is continuous phase for the all hyper-eutectic compositions even tough the volume fraction of the Si phase was lower than 30%. The hyper-eutectic compositions and their ensuing undercooling at the liquid–solid interface could not produce a wholly eutectic structure without formation of primary crystals of YSi_2. The higher solidification rates forced the primary YSi_2-phase to bifurcation. The necessary condition to produce a wholly eutectic structure through formation a *coupled zone* at the YSi_2-rich region of Si–YSi_2-eutectic alloy could not be realized.

4. Discussion

The directional solidification of diphasic structures is a simple method that can be termed as “natural lithography”. During solidification, each component partitions to produce localized equilibrium phases which minimizes the interfacial energy between the phases and lowers the Gibbs’ free energy of the whole system to accommodate the departure from the equilibrium. The departure from the equilibrium is produced through temperature gradients and constitutional supercooling produced by compositional difference from the equilibrium condition at the liquid–solid interface. This partitioning of the constituents repeats itself in a fixed frequency which depends on the interdiffusion coefficient of the components. The directional solidification of a eutectic is in a sense merge of “top-down” and “bottom-up” process. It is “top-down” process because we have control of the lamellar and rod spacing by simply controlling the ratio of the pull-rate to the imposed thermal gradient. It is a “bottom-up process” because the partitioning and assembly of atoms is self directed. This produces self-assemble structures of rods or lamella depending on the interfacial energetics and phase transition kinetics. Such a massively parallel and precise self-assembly of two-dimensional structures under environmentally benign processing conditions is highly attractive

Nanotechnology has created a demand for new fabrication methods with an emphasis on simple and low cost techniques. DSE is an unconventional approach compared to the low temperature biomimetic approaches. DSE has some unique advantage over biomimetic approaches. The inorganic structures derived by biomimetic strategies are often unstable in high temperature applications. Synthesis is often performed near room temperature producing fine particles that are usually metastable phases. Sintering, particle coarsening and crystallization cause the porous structure to re-organize into a stable structure. Thus, the original architectural structure is loss by thermal environments. DSE derived structures are stable in thermal environments since they are derived from a high temperature process.

Lithographic technology is matured for silicon based technology. Dimensional aspect ratios are limited in semiconducting materials because the anisotropic etch properties are controlled by crystallography. DSE offers the potential to fabricate structures with high aspect ratios (height to width on the order of 1000:1) utilizing the anisotropic etched behavior between phases. Our experiments in the Si–$TiSi_2$ system have successfully etched away Si exposing the $TiSi_2$ structure. DSE offers an alternative method in fabricating high aspect ratio structures for non-silicon base materials.

Not all eutectic systems solidify into a lamellar or rod microstructure as shown with the Si–YSi_2 system. Thus, material selection for specific applications is limited to systems that exhibit lamellar and rod structures. However, DSE offers a range of material selection from metal systems, ceramic systems and metal–ceramic systems. Like other bottom-up methods, DSE is not suitable to make complex or interconnected patterns.

One of the technical challenges for DSE is to bridge the nanoscopic and macroscopic worlds. In DSE, periodic ordering of the minor phase can range from 100 nm to 100 μm

depending on the system and phase content. The architectural structure for solidification is dependent upon strong chemical bonding between atoms. Constituents partition into atomic level arrangements at the liquid–solid interface to form polyphase structures. This atomic level arrangement at the liquid–solid interface is controlled by the atomic diffusion and total undercooling due to composition (diffusion), kinetics and curvature of the boundary phases. Judicious selection of the materials system and control of the total undercooling is the key to produce structures on the nanometer scale.[14]

5. Summary

Directional solidification by the Bridgman technique was applied to the eutectic systems Si–$TiSi_2$ and Si–YSi_2. Patterned growth of $TiSi_2$ rods occurred at compositions of 70, 75 and 80 wt.% Si. Titanium reaction with BN crucible caused possible boron contamination Thermal gradient in process was insufficient to align the $TiSi_2$ rods unidirectional. Large colonies with uniform rods were observed, average rod diameter was 2.5 μm. Inter-rod spacing showed small dependence upon pull rate. Pillar arrays of $TiSi_2$ were fabricated by selective etching of Si using KOH. Dry chemical etch using a CF_4/O_2 plasma exhibit selective etching at the Si–$TiSi_2$ interface. The dry etch transforms the $TiSi_2$ rods into a pyramidal shape.

Patterned growth is not observed in the Si–YSi_2 eutectic system. Eutectic and hyper-eutectic compositions formed anomalous eutectic microstructure. Eutectic microstructure shows dependence upon the solidification rate suggesting a characteristic relationship Si phase and YSi_2 phase. Low solidification rate results in primary precipitation of YSi_2 followed by secondary formation of the eutectic structure are formed for eutectic and hyper-eutectic compositions.

Acknowledgements

This work was supported by NASA Aerospace and Power Base Nanotechnology Project, NASA Cooperative agreement NCC3-850 and Air Force Office of Scientific Research.

References

1. Dyson, F., *Scientific American*., September 1995, p. 114.
2. Ehrfeld, W., Hessel, V. and Löwe, H., *Microreactors: New Technology for Modern Chemistry*. Wiley-VCH, New York, 2000.
3. Cline, H. E., In *In Situ Composites IV*, ed. P. D. Lemkey, H. E. Cline and M. McLean. Elsevier Science Publishing Co. Inc., 1982, p. 217.
4. Angers, L. M. *et al*., In *In Situ Composites IV*, ed. P. D. Lemkey, H. E. Cline and M. McLean. Elsevier Science Publishing Co. Inc., 1982, p. 205.
5. Ditchek, B. M. and Emma, T., *Appl. Phys. Lett.*, 1984, **45**, 955.
6. Orera, V. M. *et al*., *Acta Materialia*, 2000, **48**, 4683.
7. Orera, V. M. *et al*., *Acta Physica Slovaca*, 2000, **50**, 549.
8. Wolff, L. R. *et al*., *High Temp. High Press.*, 1981, **13**, 69.
9. Hart, P. E., *Proceedings of the Conference on In-Situ Composites*. National Materials Advisory Board, National Academy of Sciences, 1973, p. 119.
10. Crossman, F. W. and Yue, A. S., *Met. Trans.*, 1971, **2**, 1545.
11. Elliott, R., *Eutectic Solidification Processing*. Butterworths & Co., London, 1983.
12. Meschel, S. and Kleppa, O., *J. Alloys Compd.*, 1998, **267**, 128.
13. Vinet, B. *et al*., *J. Colloid Interface Sci.*, 2002, **255**, 363.
14. Jackson, K. A. and Hunt, J. D., *Trans. Met. Soc. AIME*, 1966, **236**, 1129.
15. Walker, P., Tarn, W., Smolinske, S., Previato, E. and Marchisotto, E., *CRC Handbook Of Etchants For Metals*. CRC Press, Boca Raton, FL, 1990.
16. Lee, B., *J. Mater. Res.*, 1999, **14**, 1002.